A fifteen-million-year surface- and subsurface-integrated TEX$_{86}$ temperature record from the eastern equatorial Atlantic

5   Carolien M. H. van der Weijst[1], Koen J. van der Laan[1], Francien Peterse[1], Gert-Jan Reichart[1,2], Francesca Sangiorgi[1], Stefan Schouten[1,2], Tjerk J.T. Veenstra[1], Appy Sluijs[1]

[1]Department of Earth Sciences, Utrecht University, 3584 CB Utrecht, the Netherlands
[2]NIOZ Royal Netherlands Institute for Sea Research, 1797 SZ 't Horntje, the Netherlands

Correspondence to: C.M.H. van der Weijst (c.m.h.vanderweijst@uu.nl)

Abstract.

TEX$_{86}$ is a paleothermometer based on Thaumarcheotal glycerol dialkyl glycerol tetraether (GDGT) lipids and is one of the most frequently used proxies for sea-surface temperature (SST) in warmer-than-present climates. However, GDGTs are not exclusively produced in and exported from the mixed layer, so sedimentary GDGTs may contain a depth-integrated signal that

15   is also sensitive to local subsurface temperature variability. In addition, the correlation between TEX$_{86}$ and SST is not significantly stronger than that to depth-integrated mixed-layer to subsurface temperatures. The calibration of TEX$_{86}$ to SST is therefore controversial. Here we assess the influence of subsurface temperature variability on TEX86 using a downcore approach. We present a 15 Myr TEX$_{86}$ record from Ocean Drilling Program Site 959 in the Gulf of Guinea and use additional proxies to elucidate the source of the recorded TEX$_{86}$ variability. Relatively high GDGT[2/3] ratio values from 13.6 Ma

20   indicate that sedimentary GDGTs were partly sourced from deeper (>200 m) waters. Moreover, late Pliocene TEX$_{86}$ variability is highly sensitive to glacial-interglacial cyclicity, as is also recorded by benthic δ^{18}O, while the variability within dinoflagellate assemblages and surface/thermocline temperature records (U$^{k'}_{37}$ and Mg/Ca), is not primarily explained by glacial-interglacial cyclicity. Combined, these observations are best explained by TEX$_{86}$ sensitivity to sub-thermocline temperature variability. We conclude that TEX$_{86}$ represents a depth-integrated signal that incorporates a SST and a deeper component, which is

25   compatible the present-day depth distribution of Thaumarchaeota and with the GDGT[2/3] distribution in core tops. The depth-integrated TEX$_{86}$ record can potentially be used to infer SST variability, because subsurface temperature variability is generally tightly linked to SST variability. Using a subsurface calibration with peak calibration weight between 100-350 m, we estimate that east equatorial Atlantic SST cooled by ~5°C between the Late Miocene and Pleistocene. On shorter timescales, we use the TEX$_{86}$ record as a proxy for South Atlantic Central Water (SACW), which originates from surface waters in the South

30   Atlantic Gyre and mixes at depth with Antarctic Intermediate Water (AAIW). Leads and lags around the Pliocene M2 glacial (~3.3 Ma) in our record, combined with published information, suggests that the M2 glacial was marked by SACW cooling

during an austral summer insolation minimum, and that decreasing CO_2 levels were a feedback, not the initiator, of glacial expansion.

1. Introduction

35 Accurate tropical sea-surface temperature (SST) reconstructions are needed to assess oceanic heat distribution and ocean-atmosphere circulation in warmer-than-present climates, such as during the Pliocene. Tropical warming, even of a small magnitude, can lead to major changes in atmospheric circulation, with effects including intensification of monsoonal precipitation (Haywood et al., 2020; Zhang et al., 2016) and warming of the extratropics via teleconnections (Barreiro et al., 2006). At present, the most frequently used proxies for past SSTs are Mg/Ca (foraminifer calcite), $U^{k'}_{37}$ (alkenones) and TEX_{86}

40 (glycerol dialkyl glycerol tetraethers; GDGTs). Each proxy has specific confounding factors and calibration issues. For example, Mg/Ca paleothermometry requires corrections for the Mg/Ca ratio of seawater and diagenesis (Dekens et al., 2002; Evans et al., 2016), and the $U^{k'}_{37}$ proxy is insensitive to temperatures above ~28°C (Müller et al., 1998). TEX_{86} is potentially one of the best proxies to reconstruct SSTs above 28°C, but one critical concern is that GDGTs are produced by marine Thaumarchaeota throughout the water column and often dominantly below the mixed layer (Ingalls et al., 2006; Kim et al.,

45 2015; Lengger et al., 2014; Shah et al., 2008).

Although GDGTs may be dominantly produced at depths below the mixed layer, the efficiency of organic carbon export towards the sediment decreases exponentially with depth below the photic zone as shown with sediment trap data and simulations (e.g., Martin et al., 1987; Middelburg et al., 2020), which for GDGTs is supported by in situ measurements (e.g.,

50 Wüchter et al., 2005). However, as the production of GDGTs in the mixed layer is generally low relative to production within and below the thermocline, GDGTs produced below the mixed layer might still comprise a significant component of the sedimentary assemblage (e.g., Taylor et al., 2013; Ho and Laepple, 2017). The export depth of downcore GDGTs can potentially be traced with the fractional abundance of GDGT-2 to GDGT-3 (GDGT[2/3] ratio; Hernández-Sánchez et al., 2014; Pearson et al., 2016; Taylor et al., 2013; Villanueva et al., 2015). GDGT[2/3] values are typically low (<5) in suspended

55 particulate matter (SPM) sampled from shallow (<100 m) water, and sharply increase to >25 in deeper water (Hurley et al., 2018). This division is currently best explained by depth-differentiation of Thaumarcheotal ecotypes with different cyclization patterns (Kim et al., 2016; Villanueva et al., 2015). Core tops do not have GDGT[2/3] values indicative of a purely "deep" Thaumarcheotal GDGT source (Figure 1). Instead, they show a gradual transition from low to moderately high values, which can be attributed to the integration of GDGTs from a range of shallow to intermediate depths. Likewise, TEX_{86} (Equation 1)

60 may reflect a depth-integrated surface to subsurface signal (SubST), that is sensitive to temperature variability at and below the surface ocean (Kim et al., 2008, 2012; Schouten et al., 2002; Tierney and Tingley, 2015).

$$TEX_{86} = \frac{[GDGT\text{-}2 + GDGT\text{-}3 + cren']}{[GDGT\text{-}1 + GDGT\text{-}2 + GDGT\text{-}3 + cren']} \qquad (1).$$

65 Indeed, several multi-proxy paleostudies suggest that dissimilarities between TEX$_{86}$-based SST reconstructions and other temperature records may be explained by a SubST signal recorded in TEX$_{86}$ variability (e.g. Lopes dos Santos et al., 2010; McClymont et al., 2012; Rommerskirchen et al., 2011; White and Ravelo, 2020). Together with the GDGT[2/3] distribution in core tops (Figure 1), these downcore records support the use of a SubST calibration. However, the targeted depth interval and weight distribution of the temperature integration remain subject of discussion (Ho and Laepple, 2016, 2017; Tierney et

70 al., 2017). The correlation of core top TEX$_{86}$ to SST is not significantly stronger than to SubST, as obtained from a wide range of depth intervals (Ho and Laepple, 2016; Schouten et al., 2002). Therefore, the sensitivity of sedimentary TEX$_{86}$ to temperature cannot be inferred from variability in the spatial dimension but variability in the temporal dimension may provide solutions. Here, we present a new 0-15 Ma TEX$_{86}$ record from Ocean Drilling Program (ODP) Site 959 in the eastern equatorial Atlantic. We evaluate the TEX$_{86}$ and GDGT[2/3] evolution on million-year and glacial-interglacial timescales during the late

75 Pliocene. We complement these records with U$^{k'}_{37}$ SST estimates and dinoflagellate cyst (dinocyst) assemblages and compare them to the Site 959 benthic δ^{18}O record (Norris, 1998a; van der Weijst et al., 2020) and Mg/Ca-based SST and thermocline temperature records (van der Weijst et al., 2022) to elucidate the local source of downcore TEX$_{86}$-index variability and, consequently, paleoclimatic change.

2 Material and Methods

80 ### 2.1 Site, age model and sampling

ODP Site 959 was drilled during Leg 159 in the Gulf of Guinea, ~160 km offshore Ghana and Ivory Coast (3.62°N, 2.73°W; 2090 m depth; Mascle et al., 1996). It is presently located below the eastward flowing Guinea Current, which originates from the North Equatorial Counter Current and the Canary Current (Norris, 1998a). SST currently varies between 25.3-28.6°C on a seasonal time scale (Locarnini et al., 2013) and surface salinity ranges between 34.6-35.0 (Zweng et al., 2013). The water

85 column is characterized by a shallow thermocline, with the 20°C isotherm depth annually varying between ~40-60 m in response to coastal upwelling (Locarnini et al., 2013, van der Weijst et al. 2022). A minor upwelling event occurs in boreal winter and a longer and stronger event in boreal summer (Djakouré et al., 2017; Verstraete, 1992; Wiafe and Nyadjro, 2015).

We studied the 0-160 m interval of Hole C and 162-194 m interval of Hole A. The lithology gradually changes from

90 nannofossil/foraminifer chalk at the bottom to nannofossil/foraminifer ooze at the top (Mascle et al., 1996). The age model is based on nannofossil biostratigraphy (Shin et al., 1998) and benthic δ^{18}O stratigraphy (Wagner, 1998) between 0-23 mbsf, benthic δ^{18}O stratigraphy between 33-46 mbsf (van der Weijst et al., 2020), astronomical tuning of high resolution X-ray fluorescence data (Vallé et al., 2016) between 51-100 mbsf, and a spline function through planktic foraminifer and nannofossil biostratigraphy between 162-194 mbsf (Norris, 1998b; Shafik et al., 1998). We plot the data between 21.35-97.43 mbsf on the

95 revised Meters Composite Depth (rMCD) scale of Vallé et al. (2016). Because outside this interval, a splice is unavailable, we

constructed a revised Meters Below Sea Floor (rMBSF) scale in coherence with Vallé et al. (2016), assuming ~5% loss of sediment between consecutive cores (Supplementary Data Files).

The core was sampled on a relatively low resolution between 0-15 Ma for biomarker analysis and on a higher resolution in the late Pliocene (2.7-3.5 Ma) interval for multi-proxy reconstructions. A total of 219 samples were extracted for TEX_{86}, of which 105 are closely spaced in the 2.7-3.5 Ma interval. $U^{k'}_{37}$ data was generated for 79 of these samples, of which 52 from the 2.7-3.5 Ma interval. Additionally, we performed palynological assessments on 48 late Pliocene splits of samples that were also used for biomarkers analysis.

2.2 Biomarker proxies

At Utrecht University, sediment samples were freeze dried and the outer surfaces were removed using a clean knife to prevent contamination. The sediment was finely ground using a mortar and pestle. In the process, a split of coarsely ground material was taken for palynology. Biomarkers were extracted at 100 °C and 7.6 x 10^6 Pa using a dichloromethane (DCM):methanol (9:1, *v/v*) solvent mixture in an accelerated solvent extractor (ASE 350, Dionex). The total lipid extract was separated over an activated an Al_2O_3 column into an apolar, ketone and polar fraction using hexane:DCM (9:1, *v/v*), hexane:DCM (1:1, *v/v*) and DCM:methanol (1:1, *v/v*) as eluents, respectively. For GDGT analysis, a C_{46} GDGT (99 ng) standard was added to the polar fraction before it was filtered over a 0.45 µm PTFE filter and dissolved in hexane:isopropanol 99:1 (*v/v*). Measurements were performed on a Ultrahigh-Performance Liquid Chromatography-Mass Spectrometer (UHPLC-MS) using the method of Hopmans et al., (2016). Samples with a branched to isoprenoid tetraether (BIT) index of >0.3 could be influenced by terrestrially produced GDGTs (Hopmans et al., 2004; Weijers et al., 2006) and were excluded from further analysis (n=3). All samples were within the reliable range of the Methane Index (MI; Zhang et al., 2011) and Ring Index (RI; Zhang et al., 2016), suggesting no appreciable inputs from methanogenic archaea or other non-thermal factors. We will present our results using various calibrations, including the conventional approach of calibrating TEX_{86} to SST, but also using various models using the relation between TEX_{86} and various depth integrations.

The ketone fraction was dissolved in hexane and analysed on a Gas Chromatograph (GC) coupled to a flame ionisation detector (GC-FID, Hewlett Packard 6890 series) equipped with a CP-Sil 5 fused silica capillary column (25 m x 0.32 mm; film thickness 0.12 um) and a 0.53 mm precolumn. Samples were injected on-column at 70°C with helium as a carrier gas and a flow rate of 2 ml/min. The oven program was as follows: 70°C for 1 min, then ramped to 130°C at 20°C/min, then to 320°C at 4C/min, and then held isothermal for 10 mins. $U^{k'}_{37}$ values were calculated from the fractional abundances of the $C_{37:2}$ and $C_{37:3}$ alkenones following Prahl and Wakeham (1987) and calibrated to SST using the calibration of Müller et al. (1998). We chose not to adopt the Bayspline approach (Tierney and Tingley, 2018) or other tropical calibrations (e.g., Sonzogni et al. 1997 DSR

II) as it may amplify noise into signal because of difficulty in accurately determining the very small C37:3 peak areas at the high range of SST (Herbert et al., 2020).

130

2.3 Palynology

Coarsely crushed freeze-dried samples were spiked with a known amount of *Lycopodium clavatum* spores to quantify absolute palynomorph (Stockmarr, 1972) and treated with 30% HCl (2x) and 40% cold HF (2x) to remove carbonates and silicates. The residue was sieved over nylon mesh, and from the 10-250 μm fraction, the lighter organic fraction was separated from the
135 heavy mineral fraction by suspension. The remaining palynological residue was mounted on glass microscopic slides with glycerine jelly. Samples were analysed using an optical microscope at under 400× magnification and approximately 300 dinoflagellate cysts (dinocysts) were counted per sample. Taxonomy follows that of Williams et al. (2017). *Capisocysta* was only identified on the genus level, because known *Capisocysta* species are best identified by the number of antapical plates (Head, 1998), which is complicated by the common dissociation of the hypocystal plates. We calculate the relative abundances
140 of a taxon based on the total dinocyst sum. Dinocysts with affinities for cold-temperate waters in the modern ocean (Boessenkool et al., 2001; Zonneveld et al., 2013) were grouped as "cool species" and used for estimating surface water temperature. This species are: *Ataxodinium choane, Corrudinium devernaliae, Corrudinium harlandii, Impagidinium pallidum, Nematosphaeropsis labyrinthus and Pyxidinopsis reticulata*. We also use the P/(P+G) ratio (Versteegh, 1994) as a paleoproductivity index. The P/(P+G) ratio quantifies the number of cysts produced by heterotrophic dinoflagellates, which
145 are characterized by peridinioid type tabulation (P) over the total number of dinocysts, including those produced by autotrophic or mixotrophic species with a gonyaulacoid type tabulation (G).

3 Results

3.1 TEX_{86}, $U^{k'}_{37}$ and GDGT[2/3] evolution at Site 959

We explore our TEX_{86} results using several calibration approaches in Figure 2, including an SST calibration using the
150 exponential TEX_{86}^{H} (Kim et al., 2010). It should be noted that this calibration yields significant residuals in tropical regions and suffers from regression dilution (Tierney and Tingley, 2014). A linear calibration using a Bayesian method, a model for the tropical Atlantic and models assuming contributions from GDGTs produced below the mixed layer. Below, we first explore our TEX_{86} record in the context of other GDGT-based indicators and other data using the TEX_{86}^{H} calibration for SST (Figures 3-7), while subsurface calibrations are discussed in Figures 7 and 8.
155 Between 15 and 11 Ma, TEX_{86}^{H} based SST values fluctuate around an average value of ~29°C (Figure), similar to the present-day local annual maximum surface temperature of 28.6°C. A long-term gradual cooling starts around 11 Ma and is punctuated by two major cooling steps of ~2°C each, around 4.9 Ma and 3.4 Ma, in which TEX_{86}^{H} drop well below the present-day local annual minimum surface temperature of 25.3°C. The cooling trend seems to end in the late Pleistocene, where TEX_{86}^{H} records

a ~4°C warming between 0.5 Ma and present, with a core top TEX_{86}^H of 24.0°C. $U_{37}^{k'}$ is at saturation (~28°C) for most of the interval but registers some colder temperatures in the late Pliocene (27-28°C) and drops below 27°C after 1.8 Ma. The core top sample registers a temperature of 26.6°C, which is within calibration error (1.5 °C; Müller et al., 1998) of the 27.5°C modern mean annual SST (Locarnini et al., 2013). The GDGT[2/3] ratio is 7.0 in the core top. In the oldest part of the studied interval, GDGT[2/3] values vary between 4 and 5.5. Following an abrupt increase at ~13.6 Ma, GDGT[2/3] varies largely between 5 and 8. After 1.7 Ma, GDGT[2/3] persistently increases to >7.

3.2 Pliocene dinocyst assemblages

Palynological assemblages are dominated by dinocysts with only minor amounts of terrestrially derived pollen and spores. Dinocyst preservation is generally good. The assemblages are dominated by *Brigantedinium* spp. (19-60%), closely followed by *Spiniferites* spp. (8-36%) (Figure 4; see supplementary information for a complete overview of the assemblages). The interval between 3.33 Ma and 3.16 Ma was sampled at a higher resolution (~5 kyr on average) and displays strong variability of the negatively correlated *Brigantedinium* spp. and *Spiniferites* spp. on timescales <10 kyr. Other relatively abundant and consistently present taxa are *Operculodinium* spp., *Pentapharsodinium dalei* and *Impagidinium* spp. Peak abundances of *Lingulodinium* spp. were recorded at ~3.26 Ma (*Lingulodinium machaerophorum*) and at 2.77 Ma (*Lingulodinium hemicystum*). *Capisocysta* sp. is consistently present in the lower part of the interval, with peak abundances (>20%) at 3.32 Ma and 3.20 Ma but has its last occurrence at 3.17 Ma. There is general coherence between TEX_{86}^H-SST variability and the relative abundance of the "cool species" group, which is dominated by *N. labyrinthus*. On average, the dinocysts with affinities for colder-temperate waters make up 6% of the total assemblage, but peak abundances of 10-13% occur during the M2 glacial. The P/(P+G) paleoproductivity index is 0.48 on average, with minimum and maximum values of 0.23 and 0.70 respectively (Figure). It is primarily driven by the abundance of *Brigantedinium* spp. The P/(P+G) ratio shows no significant relationship with TEX_{86}^H-SST (R^2=0.05, p=0.14 in linear regression analysis).

4. Discussion

4.1 Identifying the source depth of the TEX_{86} signal

The 15-million-year TEX_{86}^H record at Site 959 shows a cooling from >30°C between 11-15 Ma to <20°C between 0-3.3 Ma (Figure). The $U_{37}^{k'}$ record, on the other hand, is near or at proxy saturation (>27°C) for most of the interval, with some lower values after 1.8 Ma. Assuming that both proxies reflect SST, the relatively small offset between $U_{37}^{k'}$ and TEX_{86}^H-SST offset in the core top sample (2.7°C) could be explained by a combination of calibration errors and seasonality. However, the average downcore offset between TEX_{86}^H and $U_{37}^{k'}$ is 5.4°C and peaks at 7-8°C during the late Pliocene interglacials (Figure 5 and Figure), which demonstrates that TEX_{86} underestimates past SST at this site, assuming that $U_{37}^{k'}$ is a more accurate representation of SST. This could potentially be resolved by using an alternative, regional SST calibration. The BAYSPAR-SST calibration (Tierney and Tingley, 2014) accounts for spatial variability of the TEX_{86}-SST relationship and is the only

190 available calibration that raises absolute SST estimates. However, similar to TEX_{86}^H (Kim et al., 2010) and low-latitude Atlantic (Zhang et al., 2018) calibrations, it likely overestimates SST variability (Figure 2), indicating that the calibration slope is too steep. This is potentially a problem inherent to the calibration of TEX_{86} to SST, and could reflect downcore TEX_{86} sensitivity to SubST instead of SST variability (Ho and Laepple, 2016). In the following sections, we explore multi-proxy data from Site 959 in search of indications for the water depth the downcore TEX_{86} signal is reflecting.

195

4.1.1 GDGT[2/3] values

A substantial contribution of GDGTs from below the oceanic surface layer is supported by the relatively high GDGT[2/3] ratio, which fluctuates between 5 and 8 in the majority of the record (Figure). Such values that are rarely observed in modern day shallow water (<100 m) SPM and surface sediments (e.g. Besseling et al., 2019; Hernández-Sánchez et al., 2014; Hurley

200 et al., 2018). These values are best explained as a mixed signal of GDGTs from the upper 200 m and intermediate waters (Figure 1c), i.e., likely dominantly from below the mixed layer (~50 m) at Site 959. A cross-plot of TEX_{86}^H-SST and GDGT[2/3] (Figure) shows that most data are clustered around a positive regression slope, but the oldest (>13.6 Ma) and youngest (<1.7 Ma) data plot outside this main cluster, potentially signaling systematic changes in GDGT production and export depth. Both 13.6 Ma and 1.7 Ma mark the onset of a strong GDGT[2/3] increase (Figure), signaling systematic

205 deepening of the source of the sedimentary GDGT signal.

The ratio of GDGT[2] to GDGT[3] in samples does not directly affect the TEX_{86}-index because they are both included in the denominator and divisor (Equation 1). If the abundance of GDGT[2] increases relative to that of GDGT[3] with export depth, then samples with a higher GDGT[2/3] ratio should be associated with lower TEX_{86} values. The positive relationship between

210 TEX_{86} and GDGT[2/3] (Figure) is therefore an interesting feature. Taylor et al. (2013) found a similar relation in the calibration data set and in the paleo-domain. Based on their analyses, they conclude that water depth is the dominant control of GDGT[2/3] ratios in sediments, recently supported by SPM analyses (Hurley et al., 2018). They also conclude that the positive correlation between SST and GDGT[2/3], notably the opposite relation to that expected based on homeoviscous adaptation, is an oceanographical artifact. Rather, the positive relation suggests that the long term TEX_{86} trends are not driven by GDGT export

215 depth but reflect overall temperature changes instead. Alternatively, non-thermal factors such as water column oxygenation and nutrient supply may have influenced GDGT cyclization: high nutrient availability and ammonia oxidation rates have been linked to low TEX_{86} values (Hurley et al., 2016; Park et al., 2018). However, following the GDGT[2/3] shift at 13.6 Ma, TEX_{86}^H does not systematically change until ~11 Ma (Figure). Moreover, late Pliocene dinocyst assemblages (Figure) are characterized by a highly variable P/(P+G) ratio, indicating that upwelling and nutrient supply were highly variable on sub-

220 Milankovitch timescales. In contrast to TEX_{86}^H (Figure 5), the P/(P+G) ratio shows no glacial-interglacial variability. It is therefore unlikely that TEX_{86} variability was primarily driven by non-thermal factors.

4.1.2 Surface, thermocline and sub-thermocline temperature variability

The late Pliocene TEX_{86}^H record follows a different evolution than SST records of $U^{k'}_{37}$ and the recent Mg/Ca of the surface
dwelling *Globigerinoides ruber* (Mg/Ca$_{(G.ruber)}$) and thermocline dwelling *Neogloboquadrina dutertrei* (Mg/Ca$_{(N.dutertrei)}$)
generated on the same samples (Figure 5). The Mg/Ca records (van der Weijst et al., 2022) are based on very well-preserved
foraminifera and applies a constant Pliocene correction for the Mg/Ca of seawater, a species-specific core top calibrations with
a constant partitioning coefficient and embedded dissolution correction (Dekens et al., 2002). Whereas TEX_{86}^H decreases by
~2°C, $U^{k'}_{37}$ and Mg/Ca-based SSTs show no significant net change in this interval. Moreover, although Mg/Ca and $U^{k'}_{37}$
register some cooling during the late Pliocene glacials, their variability seems not primarily driven by glacial-interglacial
cyclicity, as is best observed in the high-resolution interval from M2 to KM2 (Figure 5). This is also true for the relative
abundance of dinocysts with affinities for colder temperatures (Figure , Figure 5). Furthermore, around the KM2 and M2
glacials, TEX_{86}^H cooling leads increasing abundances of cool dinocysts, as well as Mg/Ca$_{(G.ruber)}$ and $U^{k'}_{37}$ cooling by ~5-10
ka (Figure), which underscores the independent evolution of these records.

At sites where TEX_{86} is suspected to be affected by GDGTs produced below the surface ocean, TEX_{86}^H has occasionally been
interpreted to reflect thermocline temperature variability (e.g. Lopes dos Santos et al., 2010). Thermocline temperatures are
lower and can be highly variable through time, which potentially explains both absolute SSTs underestimation and amplitude
overestimation in specific TEX_{86}^H records. However, both could also be explained as a general artefact of an overestimated
calibration slope that results from calibrating a depth-integrated GDGT signal to SST (Ho and Laepple, 2015, 2016). Our
TEX_{86}^H record shows weak coherence with the Site 959 Mg/Ca$_{(N.dutertrei)}$ thermocline temperature record (Figure 5; van der
Weijst et al., 2022). Whereas TEX_{86} registers late Pliocene cooling, Mg/Ca$_{(N. dutertrei)}$ registers warming in relation to
thermocline deepening (van der Weijst et al., 2022). Moreover, while the range of Mg/Ca$_{(N. dutertrei)}$ temperatures is similar to
TEX_{86}^H on glacial-interglacial timescales, Mg/Ca$_{(N. dutertrei)}$ does not follow the glacial-interglacial cyclicity as recorded in the
TEX_{86}.

In contrast, the variability in the TEX_{86}^H-SST and benthic $\delta^{18}O$ records at Site 959 is very similar (Figure 3, Figure 5). Benthic
$\delta^{18}O$ is a faithful recorder of glacial-interglacial cyclicity because it registers a combined signal of deep ocean temperature and
polar ice sheet volume. Could TEX_{86} at Site 959 also be sensitive to glacial-interglacial cyclicity in deeper waters? At the onset
of the M2 and KM2 glacials, the glacial expression of TEX_{86}^H leads $\delta^{18}O$ by ~5 kyr (Figure), which indicates that, despite the
similarities between TEX_{86}^H-SST and benthic $\delta^{18}O$, these proxies record variability in different water masses. Bottom waters
at Site 959 are predominantly ventilated by North Atlantic Deep Water (NADW), whereas depths below the thermocline are
occupied by South Atlantic Central Water (SACW; Figure). SACW originates from surface waters in the South Atlantic gyre,
which at depth mixes with Antarctic Intermediate Water (AAIW). It is therefore sensitive to climate variability in the mid-
latitudes in the southern hemisphere and, like benthic $\delta^{18}O$, sensitive to higher-latitude climate change. Although our record

samples SACW, AAIW dynamics have previously been suggested to be the main driver of TEX_{86} variability in the Arabian Sea (Huguet et al., 2006) and in the southeast Atlantic (Rommerskirchen et al., 2011). If TEX_{86} at Site 959 records a mixed signal from surface and subsurface waters, as is supported by the relatively high GDGT[2/3] ratio (Figure 1 and Figure), it is likely sensitive to SACW dynamics, which explains the strong coherence with the benthic $\delta^{18}O$ record. Collectively, these observations suggests that the downcore TEX_{86} record at Site 959 is substantially affected by temperature variability below the surface ocean, and that calibration to SubST is more appropriate than to SST.

4.2 Calibration of the depth-integrated TEX_{86} record

Several TEX_{86}-SubST calibrations are available, with each assuming, among other things, a different depth-integration of the water column (Figure). The BAYSPAR-SubST (Tierney and Tingley, 2014) and TEX_{86}^{H}-SubST (Kim et al., 2012) calibrations both target the upper 200 m of the water column, but the weight of the BAYSPAR-SubST calibration is centered at relatively shallow depths compared to the linearly weighted TEX_{86}^{H}-SubST calibration (Figure). The HL16-SubST (Ho and Laepple, 2016) calibration targets the upper 950 m. The validity of this depth interval was questioned (Tierney et al., 2017), but with peak calibration weight at 100-350 m (Figure), it is compatible with the documented vertical distribution of Thaumarcheotal cells counts and GDGT concentrations (e.g. Hernández-Sánchez et al., 2014; Schouten et al., 2012; Wuchter et al., 2005; Sintes et al. 2016), leaving export efficiency as the major uncertainty. Moreover, based on the large proportion of core tops with higher (>5) GDGT[2/3] values in the global calibration set (Figure 1), a slightly deeper calibration target (including depths below 200 m) is arguably preferable. This deeper calibration target lowers the slope of the calibration, which dampens reconstructed Miocene-Pliocene temperature variability at Site 959 (Figure 2).

The ratio between temperature change in the surface and subsurface ocean is 1:1 when averaged across many sites and on longer timescales (Ho and Laepple, 2016). Under the assumption that the (integrated) depth of GDGT sourcing and the structure of the water column was stable, a depth-integrated TEX_{86} record might still be of value to assess SST variability. Depending on the calibration, the magnitude of Late Miocene to Pleistocene cooling at Site 959 is 10°C (BAYSPAR-SubST), 7°C (TEX_{86}^{H}-SubST) or 5°C (HL16-SubST; Figure 8). Assuming a 1:1 ratio, the long-term SST trend should be of a similar magnitude. Currently available tropical SST estimates on the studied timescale are either compromised by saturation of the $U^{k'}_{37}$ proxy, or are based on TEX_{86}, and are therefore not suitable for independent comparison. However, global mean surface temperature estimates based on benthic $\delta^{18}O$ data suggest a ~5°C cooling across the same interval (Hansen et al., 2013; Tierney et al., 2020). In the absence of major oceanographic changes, it is unlikely that the local cooling trend at Site 959 was larger, because temperature variability is generally lower in the tropics compared to high latitudes where deep-ocean waters derive from (i.e., polar amplification). This suggests that the BAYSPAR-SubST and TEX_{86}^{H}-SubST calibrations may overestimate the magnitude of long-term cooling (Figure). From the currently available calibrations, HL16-SubST best approximates both expected glacial-interglacial variability and multi-million year trends (Figure 2, Figure), and could potentially be used in

combination with other SST records and/or modern water column data to correct for the local SST-SubST offset (Figure 2). It is possible that the 1:1 ratio between SST and SubST did not persist across the entire record, e.g., due to changes in SACW production. To further improve tropical SST estimates in warmer climates, it should be further explored under which conditions a TEX_{86} record that is driven by subsurface variability can be used to reconstruct SST variability, and how to correct for the surface-subsurface temperature offset.

4.3 Late Neogene TEX_{86} as an intermediate ocean signal at Site 959: New insights in M2 glacial inception

It is currently unclear what caused M2 glacial inception, but hypothesized mechanisms include declining atmospheric CO_2 levels (Berends et al., 2019; Dolan et al., 2015), reduced latitudinal heat transport by the North Atlantic Current (de Schepper et al., 2009; 2013) on the Northern Hemisphere (NH) and by Indonesian throughflow (De Vleeschouwer et al., 2018) on the Southern Hemisphere (SH). Multi-proxy data from Site 999 in the Caribbean Sea show that declining CO_2 levels lagged the benthic $\delta^{18}O$ glacial expression at the onset of M2 (de la Vega et al., 2020). This indicates that declining CO_2 levels did not initiate the M2 glacial, although they might have affected its intensity and duration.

Because the TEX_{86} record at Site 959 is affected by SACW, it can potentially be used to study the connection between our low-latitude site and higher latitudes. The TEX_{86} and benthic $\delta^{18}O$ records at Site 959 correspond closely but are out-of-sync during the M2 glacial (Figure). Both records, generated on the same samples, display a double peak around M2, but TEX_{86} leads $\delta^{18}O$ by ~5 kyr. Whereas the depth-integrated TEX_{86} signal at Site 959 is sensitive to SH conditions through SACW, bottom waters at Site 959 consisted predominantly of NADW sourced from the NH during the late Pliocene (van der Weijst et al., 2020). The TEX_{86} lead therefore indicates a lead of SH over NH cooling/glaciation at the onset of M2, in agreement with transient ice sheet simulation (Berends et al., 2019).

We further explore the relative chronology around M2 in Figure . The age models were aligned on peak glacial $\delta^{18}O$ values and the same records are plotted on the original age models in Figure S1. Although it is difficult to discriminate between signal and noise at this resolution, some patterns seem to emerge from this compilation. Directly before M2, benthic $\delta^{18}O$, SubST and SST records from the eastern equatorial Atlantic (Site 959 and Site 662) and Caribbean Sea (Site 999) indicate gradual, widespread cooling, while CO_2 levels were rising. A sharp drop in TEX_{86}^H-SubST indicates intermediate ocean cooling at the onset of M2, leading pronounced glacial cooling (benthic $\delta^{18}O$) of the deep ocean and tropical surface ocean (best observed at Site 662). According to the chronology in Figure , this intermediate ocean cooling occurred during a SH summer insolation minimum, suggesting that astronomical forcing may have amplified Southern Ocean cooling and tipped the system to glacial conditions. The sensitivity of the Antarctic ice sheet to astronomical forcing is also reflected by the 3.3 Ma onset of ~20 kyr cyclicity in Ice Rafted Debris (IRD) at East Antarctic Site IODP Site U1361, with peak IRD mass accumulation rates at SH summer insolation minima (Patterson et al., 2014). Based on the chronology of Figure , SH cooling led atmospheric CO_2

drawdown by ~15-20 kyr. Lags of a similar magnitude were not unusual during Pleistocene glacial inceptions (Petit et al., 1999). Marginal Antarctic diatom assemblages and lithology suggest that considerable sea ice expansion occurred during M2, which could have inhibited CO_2 outgassing from the deep ocean (Ishino and Suto, 2020; McKay et al., 2012). Moreover, a slight increase in dust-mediated iron fertilization of the Southern Ocean may have facilitated export productivity (Martínez-Garcia et al., 2011). In combination with reduced mixing between Northern Component Water and Southern Component Water (van der Weijst et al., 2020), these processes would have led to increased carbon storage in the deep ocean in response to M2 cooling. Higher resolution records and correlations would be required to fully test this hypothesis.

5. Conclusions

Several lines of evidence show that the TEX_{86} record at Site 959 in the eastern equatorial Atlantic is best explained as a depth-integrated signal that is substantially affected by temperature variability below the thermocline. Relatively high GDGT[2/3] ratios since ~13.6 Ma indicate that the sedimentary GDGTs were partly sourced from deeper (>200 m) waters. Moreover, late Pliocene multi-proxy data shows that TEX_{86} variability is predominantly driven by glacial-interglacial variability, in contrast to other SST and thermocline records ($U^{k'}_{37}$ and $Mg/Ca_{(G.ruber)}$ SST and $Mg/Ca_{(N.duterrei)}$) and dinocyst abundances. The TEX_{86} record strongly resembles the benthic $\delta^{18}O$ record, indicating that it dominantly records temperature changes in a sub-thermocline water mass. At Site 959, intermediate depths are occupied by SACW, which derives from the mid latitudes of the South Atlantic. According to the present-day water column composition, a substantial contribution of GDGTs from deeper (>200) waters is needed to obtain TEX_{86} sensitivity to SACW. This favors a subsurface calibration that integrates across a wider range of water depths, such as HL16-SubST (Ho & Laepple, 2016), in which calibration weight peaks 100-350 m. This calibration target interval is compatible with pelagic Thaumarcheotal cell counts and GDGT concentrations, and with core top GDGT[2/3] values in the global calibration set.

Even if TEX_{86} mainly relects SubST variability, it may be a used to reconstuct past SSTs if the temporal relationship between SST-SubST in a certain region is well-understood. Assuming a 1:1 relationship between long-term SubST and SST trends, our TEX_{86} record suggests 5°C tropical SST cooling between the Late Miocene and Pleistocene when calibrated with HL16-SubST. Additionally, TEX_{86} is also highly informative as a SubST proxy, because the sensitivity of TEX_{86} to SACW at Site 959 offers a chance to explore connections between high and low latitude climate variability. The TEX_{86} and benthic $\delta^{18}O$ records at Site 959 are highly similar, but TEX_{86} is sensitive to high latitude SH conditions through AAIW, whereas the benthic $\delta^{18}O$ record is primarily forced by high latitude NH conditions through NADW. A ~5 kyr lead of TEX_{86} relative to $\delta^{18}O$ at the onset of the M2 glacial stage indicates a lead of SH over NH cooling. Albeit limited by the resolution of the datasets, multi-proxy data from Site 959, Site 999 (Caribbean Sea) and Site 662 (eastern equatorial Atlantic) aligned based on LR04 peak glacial $\delta^{18}O$ values indicate that SH cooling also led tropical ocean cooling and CO_2 levels by 15-20 kyr, suggesting that CO_2

drawdown was a consequence of glacial conditions. Instead, glacial expansion and SACW cooling at SH insolation minima suggest that orbital forcing played a pivotal role in M2 glacial inception.

Data availability

New Site 959 data are available as a supplement to this paper and will be uploaded to the PANGAEA online data repository upon publication.

Competing interests

The authors declare that they have no conflict of interest.

Acknowledgements

We thank the International Ocean Discovery Program and the predecessor drilling programs for samples and data. We thank Arnold van Dijk, Giovanni Dammers, Natasja Welters, Klaas van Nierop and Dominika Kasjaniuk (Utrecht University) and Wim Boer (NIOZ) for analytical support. This work was carried out under the program of the Netherlands Earth System Science Centre (NESSC), financially supported by the Ministry of Education, Culture and Science (OCW). AS thanks the European Research Council for Consolidator Grant 771497.

References

Barreiro, M., Philander, S. G., Pacanowski, R. and Fedorov, A. V.: Simulations of warm tropical conditions with application to middle Pliocene atmospheres, Clim. Dyn., 26(4), 349–365, doi:10.1007/s00382-005-0086-4, 2006.

Berends, C. J., de Boer, B., Dolan, A. M., Hill, D. J. and van de Wal, R. S. W.: Modelling ice sheet evolution and atmospheric CO2 during the Late Pliocene, Clim. Past, 15(4), 1603–1619, doi:10.5194/cp-15-1603-2019, 2019.

Besseling, M. A., Hopmans, E. C., Koenen, M., van der Meer, M. T. J., Vreugdenhil, S., Schouten, S., Sinninghe Damsté, J. S. and Villanueva, L.: Depth-related differences in archaeal populations impact the isoprenoid tetraether lipid composition of the Mediterranean Sea water column, Org. Geochem., 135, 16–31, doi:10.1016/j.orggeochem.2019.06.008, 2019.

Boessenkool, K. P., Van Gelder, M. J., Brinkhuis, H. and Troelstra, S. R.: Distribution of organic-walled dinoflagellate cysts in surface sediments from transects across the Polar Front offshore Southeast Greenland, J. Quat. Sci., 16(7), 661–666, doi:10.1002/jqs.654, 2001.

Dekens, P. S., Lea, D. W., Pak, D. K. and Spero, H. J.: Core top calibration of Mg/Ca in tropical foraminifera: Refining paleotemperature estimation, Geochemistry, Geophys. Geosystems, 3(4), 1–29, doi:10.1029/2001GC000200, 2002.

Djakouré, S., Penven, P., Bourlès, B., Koné, V. and Veitch, J.: Respective roles of the Guinea current and local winds on the coastal upwelling in the northern Gulf of Guinea, J. Phys. Oceanogr., 47(6), 1367–1387, doi:10.1175/JPO-D-16-0126.1, 2017.

Dolan, A. M., Haywood, A. M., Hunter, S. J., Tindall, J. C., Dowsett, H. J., Hill, D. J. and Pickering, S. J.: Modelling the enigmatic Late Pliocene Glacial Event - Marine Isotope Stage M2, Glob. Planet. Change, 128, 47–60, doi:10.1016/j.gloplacha.2015.02.001, 2015.

Evans, D., Brierley, C. M., Raymo, M. E., Erez, J. and Müller, W.: Planktic foraminifera shell chemistry response to seawater chemistry: Pliocene–Pleistocene seawater Mg/Ca, temperature and sea level change, Earth Planet. Sci. Lett., 438, 139–148, doi:10.1016/j.epsl.2016.01.013, 2016.

Hansen, J., Sato, M., Russell, G. and Kharecha, P.: Climate sensitivity, sea level and atmospheric carbon dioxide, Philos. Trans. R. Soc. A Math. Phys. Eng. Sci., 371(2001), 20120294, doi:10.1098/rsta.2012.0294, 2013.

Haug, G. H., Tiedemann, R., Zahn, R. and Ravelo, A. C.: Role of Panama uplift on oceanic freshwater balance, Geology, 29(3), 207–210, doi:10.1130/0091-7613(2001)029<0207:ROPUOO>2.0.CO;2, 2001.

Haywood, A. M., Tindall, J. C., Dowsett, H. J., Dolan, A. M., Foley, K. M., Hunter, S. J., Hill, D. J., Chan, W. Le, Abe-Ouchi, A., Stepanek, C., Lohmann, G., Chandan, D., Richard Peltier, W., Tan, N., Contoux, C., Ramstein, G., Li, X., Zhang, Z., Guo, C., Nisancioglu, K. H., Zhang, Q., Li, Q., Kamae, Y., Chandler, M. A., Sohl, L. E., Otto-Bliesner, B. L., Feng, R., Brady, E. C., Von Der Heydt, A. S., Baatsen, M. L. J. and Lunt, D. J.: The Pliocene Model Intercomparison Project Phase 2: Large-scale climate features and climate sensitivity, Clim. Past, 16(6), 2095–2123, doi:10.5194/cp-16-2095-2020, 2020.

Head, M. J.: New goniodomacean dinoflagellates with a compound hypotractal archeopyle from the late cenozoic: Capisocysta Warny and Wrenn, emend., J. Paleontol., 72(5), 797–809, doi:10.1017/S0022336000027153, 1998.

Herbert, T. D., Peterson, L. C., Lawrence, K. T. and Liu, Z.: Tropical ocean temperatures over the past 3.5 million years., Science (80-.)., 328(5985), 1530–1534, doi:10.1126/science.1185435, 2010.

Hernández-Sánchez, M. T., Woodward, E. M. S., Taylor, K. W. R., Henderson, G. M. and Pancost, R. D.: Variations in GDGT distributions through the water column in the South East Atlantic Ocean, Geochim. Cosmochim. Acta, 132(May), 337–348, doi:10.1016/j.gca.2014.02.009, 2014.

Hertzberg, J. E., Schmidt, M. W., Bianchi, T. S., Smith, R. K., Shields, M. R. and Marcantonio, F.: Comparison of eastern tropical Pacific TEX86 and Globigerinoides ruber Mg/Ca derived sea surface temperatures: Insights from the Holocene and Last Glacial Maximum, Earth Planet. Sci. Lett., 434, 320–332, doi:10.1016/j.epsl.2015.11.050, 2016.

Ho, S. L. and Laepple, T.: Glacial cooling as inferred from marine temperature proxies TEXH86and UK'37, Earth Planet. Sci. Lett., 409, 15–22, doi:10.1016/j.epsl.2014.10.033, 2015.

Ho, S. L. and Laepple, T.: Flat meridional temperature gradient in the early Eocene in the subsurface rather than surface ocean, Nat. Geosci., 9(August), doi:10.1038/ngeo2763, 2016.

Ho, S. L. and Laepple, T.: Reply to "Eocene temperature gradients," Nat. Geosci., 10(8), 539–540, doi:10.1038/ngeo2998, 2017.

Holbourn, A., Kuhnt, W., Frank, M. and Haley, B. a.: Changes in Pacific Ocean circulation following the Miocene onset of permanent Antarctic ice cover, Earth Planet. Sci. Lett., 365, 38–50, doi:10.1016/j.epsl.2013.01.020, 2013.

Hopmans, E. C., Weijers, J. W. H., Schefuß, E., Herfort, L., Sinninghe Damsté, J. S. and Schouten, S.: A novel proxy for terrestrial organic matter in sediments based on branched and isoprenoid tetraether lipids, Earth Planet. Sci. Lett., 224(1–2), 107–116, doi:10.1016/j.epsl.2004.05.012, 2004.

Huguet, C., Kim, J. H., Damsté, J. S. S. and Schouten, S.: Reconstruction of sea surface temperature variations in the Arabian Sea over the last 23 kyr using organic proxies (TEX86 and U 37K'), Paleoceanography, 21(3), 1–13, doi:10.1029/2005PA001215, 2006.

Hurley, S. J., Elling, F. J., Könneke, M., Buchwald, C., Wankel, S. D. and Santoro, A. E.: Influence of ammonia oxidation rate on thaumarchaeal lipid composition and the TEX 86 temperature proxy, , 113(28), 7762–7767, doi:10.1073/pnas.1518534113, 2016.

Hurley, S. J., Lipp, J. S., Close, H. G., Hinrichs, K. U. and Pearson, A.: Distribution and export of isoprenoid tetraether lipids in suspended particulate matter from the water column of the Western Atlantic Ocean, Org. Geochem., 116, 90–102, doi:10.1016/j.orggeochem.2017.11.010, 2018.

Ingalls, A. E., Shah, S. R., Hansman, R. L., Aluwihare, L. I., Santos, G. M., Druffel, E. R. M. and Pearson, A.: Quantifying archaeal community autotrophy in the mesopelagic ocean usinq natural radiocarbon, Proc. Natl. Acad. Sci. U. S. A., 103(17), 6442–6447, doi:10.1073/pnas.0510157103, 2006.

Ishino, S. and Suto, I.: Late Pliocene sea-ice expansion and its influence on diatom species turnover in the Southern Ocean, Mar. Micropaleontol., 160(June 2019), 101895, doi:10.1016/j.marmicro.2020.101895, 2020.

Kim, J.-H., van der Meer, J., Schouten, S., Helmke, P., Willmott, V., Sangiorgi, F., Koç, N., Hopmans, E. C. and Damsté, J. S. S.: New indices and calibrations derived from the distribution of crenarchaeal isoprenoid tetraether lipids: Implications for past sea surface temperature reconstructions, Geochim. Cosmochim. Acta, 74(16), 4639–4654, doi:10.1016/j.gca.2010.05.027, 2010.

Kim, J.-H., Romero, O. E., Lohmann, G., Donner, B., Laepple, T., Haam, E. and Sinninghe Damsté, J. S.: Pronounced subsurface cooling of North Atlantic waters off Northwest Africa during Dansgaard–Oeschger interstadials, Earth Planet. Sci. Lett., 339–340, 95–102, doi:10.1016/j.epsl.2012.05.018, 2012.

Kim, J. H., Schouten, S., Hopmans, E. C., Donner, B. and Sinninghe Damsté, J. S.: Global sediment core-top calibration of the TEX86 paleothermometer in the ocean, Geochim. Cosmochim. Acta, 72(4), 1154–1173, doi:10.1016/j.gca.2007.12.010, 2008.

Kim, J. H., Schouten, S., Rodrigo-Gámiz, M., Rampen, S. W., Marino, G., Huguet, C., Helmke, P., Buscail, R., Hopmans, E. C., Pross, J., Sangiorgi, F., Middelburg, J. B. M. and Sinninghe Damsé, J. S.: Influence of deep-water derived isoprenoid tetraether lipids on the TEX86H paleothermometer in the Mediterranean Sea, Geochim. Cosmochim. Acta, 150, 125–141, doi:10.1016/j.gca.2014.11.017, 2015.

Kim, J. H., Villanueva, L., Zell, C. and Sinninghe Damsté, J. S.: Biological source and provenance of deep-water derived isoprenoid tetraether lipids along the Portuguese continental margin, Geochim. Cosmochim. Acta, 172, 177–204, doi:10.1016/j.gca.2015.09.010, 2016.

Martin, J. H., Knauer, G. A., Karl, D. M., and Broenkow, W. W.: VERTEX: carbon cycling in the northeast Pacific, Deep Sea Research Part A, Oceanographic Research Papers, 34(2), 267-285, doi.org/10.1016/0198-0149(87)90086-0, 1987.

Middelburg, J. J.: Marine Carbon Biogeochemistry, Springer Briefs in Earth System Sciences, 1, https://doi.org/10.1007/978-3-030-10822-9_1, 2019.

435   Laskar, J.: The chaotic motion of the solar system: A numerical estimate of the size of the chaotic zones, Icarus, doi:10.1016/0019-1035(90)90084-M, 1990.

Lengger, S. K., Hopmans, E. C., Sinninghe Damsté, J. S. and Schouten, S.: Impact of sedimentary degradation and deep water column production on GDGT abundance and distribution in surface sediments in the Arabian Sea: Implications for the TEX86 paleothermometer, Geochim. Cosmochim. Acta, 142, 386–399, doi:10.1016/j.gca.2014.07.013, 2014.

Li, D., Zhao, M., Tian, J. and Li, L.: Comparison and implication of TEX86 and U37K' temperature records over the last 356kyr of ODP Site 1147 from the
440   northern South China Sea, Palaeogeogr. Palaeoclimatol. Palaeoecol., 376, 213–223, doi:10.1016/j.palaeo.2013.02.031, 2013.

Lisiecki, L. E. and Raymo, M. E.: A Pliocene-Pleistocene stack of 57 globally distributed benthic δ 18 O records, Paleoceanography, 20(1), doi:10.1029/2004PA001071, 2005.

Locarnini, R. A., Mishonov, A. V., Antonov, J. I., Boyer, T. P., Garcia, H. E., Baranova, O. K., Zweng, M. M., Paver, C. R., Reagan, J. R., Johnson, D. R., Hamilton, M. and Seidov, D.: World Ocean Atlas 2013. Vol. 1: Temperature., S. Levitus, Ed.; A. Mishonov, Tech. Ed.; NOAA Atlas NESDIS, 73(September),
445   40, doi:10.1182/blood-2011-06-357442, 2013.

Lopes dos Santos, R. A., Prange, M., Castañeda, I. S., Schefuß, E., Mulitza, S., Schulz, M., Niedermeyer, E. M., Sinninghe Damsté, J. S. and Schouten, S.: Glacial-interglacial variability in Atlantic meridional overturning circulation and thermocline adjustments in the tropical North Atlantic, Earth Planet. Sci. Lett., 300(3–4), 407–414, doi:10.1016/j.epsl.2010.10.030, 2010.

Martínez-Garcia, A., Rosell-Melé, A., Jaccard, S. L., Geibert, W., Sigman, D. M. and Haug, G. H.: Southern Ocean dust–climate coupling over the past four
450   million years, Nature, 476(7360), 312–315, doi:10.1038/nature10310, 2011.

Mascle, J., Lohmann, G., Clift, P. D. and and the shipboard scientific party: Proceedings of the Ocean Drilling Program, Initial Reports 159, Proc. Ocean Drill. Program, Initial Reports, 159(College Station, TX, Ocean Drilling Program), 1996.

McClymont, E. L., Ganeshram, R. S., Pichevin, L. E., Talbot, H. M., Van Dongen, B. E., Thunell, R. C., Haywood, A. M., Singarayer, J. S. and Valdes, P. J.: Sea-surface temperature records of Termination 1 in the Gulf of California: Challenges for seasonal and interannual analogues of tropical Pacific climate
455   change, Paleoceanography, 27(2), doi:10.1029/2011PA002226, 2012.

McKay, R., Naish, T., Carter, L., Riesselman, C., Dunbar, R., Sjunneskog, C., Winter, D., Sangiorgi, F., Warren, C., Pagani, M., Schouten, S., Willmott, V., Levy, R., DeConto, R. and Powell, R. D.: Antarctic and Southern Ocean influences on Late Pliocene global cooling, Proc. Natl. Acad. Sci., 109(17), 6423–6428, doi:10.1073/pnas.1112248109, 2012.

Müller, P. J., Kirst, G., Ruhland, G., Von Storch, I. and Rosell-Melé, A.: Calibration of the alkenone paleotemperature index U37K based on core-tops from
460   the eastern South Atlantic and the global ocean (60°N-60°S), Geochim. Cosmochim. Acta, 62(10), 1757–1772, doi:10.1016/S0016-7037(98)00097-0, 1998.

Norris, R.D.: Miocene-Pliocene surface-water hydrography of the eastern equatorial Atlantic. In: Mascle, J., Lohmann, G.P., Moullade, M. (eds.), Proceedings of the Ocean Drilling Program, Scientific Results Vol. 159, College Station, TX (Ocean Drilling Program), 539-555, doi:10.2973/odp.proc.sr.159.021, 1998a.

Norris, R.D.: Planktonic foraminifer biostratigraphy: Eastern equatorial Atlantic. In: Mascle, J., Lohmann, G.P., Moullade, M. (eds.), Proceedings of the Ocean Drilling Program, Scientific Results Vol. 159, College Station, TX (Ocean Drilling Program), 445-479, doi: 10.2973/odp.proc.sr.159.036.1998, 1998b.

465   Park, E., Hefter, J., Fischer, G. and Mollenhauer, G.: TEX86 in sinking particles in three eastern Atlantic upwelling regimes, Org. Geochem., 124, 151–163, doi:10.1016/j.orggeochem.2018.07.015, 2018.

Patterson, M. O., McKay, R., Naish, T. R., Escutia, C., Jimenez-Espejo, F. J., Raymo, M. E., Meyers, S. R., Tauxe, L., Brinkhuis, H. and Scientists, I. E. 318: Orbital forcing of the East Antarctic ice sheet during the Pliocene and Early Pleistocene, Nat. Geosci, 7(11), 841–847, doi:10.1038/ngeo2273, 2014.

Pearson, A., Hurley, S. J., Walter, S. R. S., Kusch, S., Lichtin, S. and Zhang, Y. G.: Stable carbon isotope ratios of intact GDGTs indicate heterogeneous
470   sources to marine sediments, Geochim. Cosmochim. Acta, 181, 18–35, doi:10.1016/j.gca.2016.02.034, 2016.

Petit, J. R., Jouzel, J., Raynaud, D., Barkov, N. I., Barnola, J.-M., Basile, I., Bender, M., Chappellaz, J., Davisk, M., Delaygue, G., Delmotte, M., Kotlyakov, V. M., Legrand, M., Lipenkov, V. Y., Lorius, C., Pé, L., Ritz, C., Saltzmank, E. and Stievenard, M.: Climate and atmospheric history of the past 420,000 years from the Vostok ice core, Antarctica The recent completion of drilling at Vostok station in East, Nature, 399, 429–436 [online] Available from: www.nature.com, 1999.

475   Plancq, J., Grossi, V., Pittet, B., Huguet, C., Rosell-Melé, A. and Mattioli, E.: Multi-proxy constraints on sapropel formation during the late Pliocene of central Mediterranean (southwest Sicily), Earth Planet. Sci. Lett., 420(April), 30–44, doi:10.1016/j.epsl.2015.03.031, 2015.

Prahl, F. G. and Wakeham, S. G.: Calibration of unsaturation patterns in long-chain ketone compositions for palaeotemperature assessment, Nature, 330(6146), 367–369, doi:10.1038/330367a0, 1987.

Rommerskirchen, F., Condon, T., Mollenhauer, G., Dupont, L. and Schefuss, E.: Miocene to Pliocene development of surface and subsurface temperatures in
480   the Benguela Current system, Paleoceanography, 26(3), 1–15, doi:10.1029/2010PA002074, 2011.

Schepper, S. De, Head, M. J. and Groeneveld, J.: North Atlantic Current variability through marine isotope stage M2 (circa 3.3 Ma) during the mid-Pliocene, Paleoceanography, 24(4), doi:10.1029/2008PA001725, 2009.

De Schepper, S., Groeneveld, J., Naafs, B. D. a., Van Renterghem, C., Hennissen, J., Head, M. J., Louwye, S. and Fabian, K.: Northern Hemisphere Glaciation during the Globally Warm Early Late Pliocene, edited by V. C. Smith, PLoS One, 8(12), e81508, doi:10.1371/journal.pone.0081508, 2013.

485 Schouten, S., Hopmans, E. C., Schefuß, E. and Sinninghe Damsté, J. S.: Distributional variations in marine crenarchaeotal membrane lipids: a new tool for reconstructing ancient sea water temperatures?, Earth Planet. Sci. Lett., 204, 265–274 [online] Available from: http://www.sciencedirect.com/science/article/pii/S0012821X02009792 (Accessed 5 February 2013), 2002.

Schouten, S., Pitcher, A., Hopmans, E. C., Villanueva, L., van Bleijswijk, J. and Sinninghe Damsté, J. S.: Intact polar and core glycerol dibiphytanyl glycerol tetraether lipids in the Arabian Sea oxygen minimum zone: I. Selective preservation and degradation in the water column and consequences for the TEX86,

490 Geochim. Cosmochim. Acta, 98, 228–243, doi:10.1016/j.gca.2012.05.002, 2012.

Seki, O., Schmidt, D. N., Schouten, S., Hopmans, E. C., Sinninghe Damsté, J. S. and Pancost, R. D.: Paleoceanographic changes in the Eastern Equatorial Pacific over the last 10 Myr, Paleoceanography, 27(3), n/a-n/a, doi:10.1029/2011PA002158, 2012.

Shafik, S., Watkins, D. K. and Shin, I. C.: Upper Cenozoic calcareous nannofossil biostratigraphy, Cote d'Ivoire-Ghana Margin, eastern equatorial Atlantic, Proc. Ocean Drill. Progr. Sci. Results, 159, 509–523, doi:10.2973/odp.proc.sr.159.022.1998, 1998.

495 Shah, S. R., Mollenhauer, G., Ohkouchi, N., Eglinton, T. I. and Pearson, A.: Origins of archaeal tetraether lipids in sediments: Insights from radiocarbon analysis, Geochim. Cosmochim. Acta, 72(18), 4577–4594, doi:10.1016/j.gca.2008.06.021, 2008.

Shin, I. C., Shafik, S. and Watkins, D. K.: High-resolution Pliocene-Pleistocene biostratigraphy of Site 959, eastern equatorial Atlantic Ocean, Proc. Ocean Drill. Progr. Sci. Results, 159, 533–538, 1998.

Sintes, E., De Corte, D., Haberleitner, E., and Herndl, G. J.: Geographic Distribution of Archaeal Ammonia Oxidizing Ecotypes in the Atlantic Ocean,

500 Frontiers in Microbiology, 7, doi:10.3389/fmicb.2016.00077, 2016.

Sonzogni, C., Bard, E., Rostek, F., Lafont, R., Rosell-Mele, A., and Eglinton, G.: Core-top calibration of the alkenone index vs sea surface temperature in the Indian Ocean, Deep-Sea Res. Pt. II, 44, 1445–1460, doi.org/10.1016/S0967-0645(97)00010-6, 1997.

Taylor, K. W. R., Huber, M., Hollis, C. J., Hernandez-Sanchez, M. T. and Pancost, R. D.: Re-evaluating modern and Palaeogene GDGT distributions: Implications for SST reconstructions, Glob. Planet. Change, 108(September), 158–174, doi:10.1016/j.gloplacha.2013.06.011, 2013.

505 Tierney, J. E. and Tingley, M. P.: A Bayesian, spatially-varying calibration model for the TEX86 proxy, Geochim. Cosmochim. Acta, 127, 83–106, doi:10.1016/j.gca.2013.11.026, 2014.

Tierney, J. E. and Tingley, M. P.: A TEX(8)(6) surface sediment database and extended Bayesian calibration, Sci Data, 2, 150029, doi:10.1038/sdata.2015.29, 2015.

Tierney, J. E. and Tingley, M. P.: BAYSPLINE: A new calibration for the alkenone paleothermometer, Palaeogeogr. Palaeocl., 33, 281–301,

510 doi.org/10.1002/2017PA003201, 2018.

Tierney, J. E., Poulsen, C. J., Montañez, I. P., Bhattacharya, T., Feng, R., Ford, H. L., Hönisch, B., Inglis, G. N., Petersen, S. V., Sagoo, N., Tabor, C. R., Thirumalai, K., Zhu, J., Burls, N. J., Foster, G. L., Goddéris, Y., Huber, B. T., Ivany, L. C., Turner, S. K., Lunt, D. J., McElwain, J. C., Mills, B. J. W., Otto-Bliesner, B. L., Ridgwell, A. and Zhang, Y. G.: Past climates inform our future, Science (80-.), 370(6517), doi:10.1126/science.aay3701, 2020.

Vallé, F., Westerhold, T. and Dupont, L.: Orbital-driven environmental changes recorded at ODP Site 959 (eastern equatorial Atlantic) from the Late Miocene

515 to the Early Pleistocene, Int. J. Earth Sci., 106(3), 1161–1174, doi:10.1007/s00531-016-1350-z, 2016.

de la Vega, E., Chalk, T. B., Wilson, P. A., Bysani, R. P. and Foster, G. L.: Atmospheric CO2 during the Mid-Piacenzian Warm Period and the M2 glaciation, Sci. Rep., 10(1), 11002, doi:10.1038/s41598-020-67154-8, 2020.

Versteegh, G. J. M.: Recognition of cyclic and non-cyclic environmental changes in the Mediterranean Pliocene: A palynological approach, Mar. Micropaleontol., 23(2), 147–183, doi:10.1016/0377-8398(94)90005-1, 1994.

520 Verstraete, J. M.: The seasonal upwellings in the Gulf of Guinea, Prog. Oceanogr., 29(1), 1–60, doi:10.1016/0079-6611(92)90002-H, 1992.

Villanueva, L., Schouten, S. and Sinninghe Damsté, J. S.: Depth-related distribution of a key gene of the tetraether lipid biosynthetic pathway in marine Thaumarchaeota, Environ. Microbiol., 17(10), 3527–3539, doi:10.1111/1462-2920.12508, 2015.

De Vleeschouwer, D., Auer, G., Smith, R., Bogus, K., Christensen, B., Groeneveld, J., Petrick, B., Henderiks, J., Castañeda, I. S., O'Brien, E., Ellinghausen, M., Gallagher, S. J., Fulthorpe, C. S. and Pälike, H.: The amplifying effect of Indonesian Throughflow heat transport on Late Pliocene Southern Hemisphere

525 climate cooling, Earth Planet. Sci. Lett., 500, 15–27, doi:10.1016/j.epsl.2018.07.035, 2018.

Wagner, T.: Pliocene-Pleistocene deposition of carbonate and organic carbon at Site 959: Paleoenvironmental implications for the eastern equatorial Atlantic off the Ivory Coast/Ghana. In: Mascle, J., Lohmann, G.P., Moullade, M. (eds.), Proceedings of the Ocean Drilling Program, Scientific Results Vol. 159, College Station, TX (Ocean Drilling Program), 557-574, doi:10.2973/odp.proc.sr.159.018.1998, 1998.

Weijers, J. W. H., Schouten, S., Spaargaren, O. C. and Sinninghe Damsté, J. S.: Occurrence and distribution of tetraether membrane lipids in soils: Implications

530 for the use of the TEX86 proxy and the BIT index, Org. Geochem., 37(12), 1680–1693, doi:10.1016/j.orggeochem.2006.07.018, 2006.

van der Weijst, C. M. H., Winkelhorst, J., Lourens, L., Raymo, M. E., Sangiorgi, F. and Sluijs, A.: A Ternary Mixing Model Approach Using Benthic Foraminifer δ13C-δ18O Data to Reconstruct Late Pliocene Deep Atlantic Water Mass Mixing, Paleoceanogr. Paleoclimatology, 35(12), doi:10.1029/2019PA003804, 2020.

535 van der Weijst, C. M. H., Winkelhorst, J., de Nooijer, W., von der Heydt, A., Reichart, G.-J., Sangiorgi, F., and Sluijs, A.: Pliocene evolution of the tropical Atlantic thermocline depth, Clim. Past, 18, 961–973, https://doi.org/10.5194/cp-18-961-2022, 2022..

White, S. M. and Ravelo, A. C.: The benthic B/Ca record at Site 806: new constraints on the temperature of the West Pacific Warm Pool and the "El Padre" state in the Pliocene, Paleoceanogr. Paleoclimatology, 35(10), 1–18, doi:10.1029/2019pa003812, 2020.

Wiafe, G. and Nyadjro, E. S.: Satellite observations of upwelling in the gulf of Guinea, IEEE Geosci. Remote Sens. Lett., 12(5), 1066–1070, doi:10.1109/LGRS.2014.2379474, 2015.

540 Wuchter, C., Schouten, S., Wakeham, S. G. and Sinninghe Damsté, J. S.: Temporal and spatial variation in tetraether membrane lipids of marine Crenarchaeota in particulate organic matter: Implications for TEX86 paleothermometry, Paleoceanography, 20(3), 1–11, doi:10.1029/2004PA001110, 2005.

Zhang, R., Zhang, Z., Jiang, D., Yan, Q., Zhou, X. and Cheng, Z.: Strengthened African summer monsoon in the mid-Piacenzian, Adv. Atmos. Sci., 33(9), 1061–1070, doi:10.1007/s00376-016-5215-y, 2016.

Zhang, Y. G., Zhang, C. L., Liu, X. L., Li, L., Hinrichs, K. U. and Noakes, J. E.: Methane Index: A tetraether archaeal lipid biomarker indicator for detecting 545 the instability of marine gas hydrates, Earth Planet. Sci. Lett., 307(3–4), 525–534, doi:10.1016/j.epsl.2011.05.031, 2011.

Zhang, Y. G. and Liu, X.: Export Depth of the TEX 86 Signal, Paleoceanogr. Paleoclimatology, 666–671, doi:10.1029/2018PA003337, 2018.

Zhang, Y. G., Pagani, M., & Wang, Z.: Ring Index : A new strategy to evaluate the integrity of TEX86 paleothermometry, Paleoceanography, 31(2), 220-232, doi.org/10.1002/2015PA002848, 2016.

Zonneveld, K. A. F., Marret, F., Versteegh, G., Bogus, K., Bonnet, S., Bouimetarhan, I., Crouch, E., de Vernal, A., Elshanawany, R., Edwards, L., Esper, O., 550 Forke, S., Grøsfjeld, K., Henry, M., Holzwarth, U., Kielt, J. F., Kim, S. Y., Ladouceur, S., Ledu, D., Chen, L., Limoges, A., Londeix, L., Lu, S. H., Mahmoud, M. S., Marino, G., Matsouka, K., Matthiessen, J., Mildenhal, D. C., Mudie, P., Neil, H. L., Pospelova, V., Qi, Y., Radi, T., Richerol, T., Rochon, A., Sangiorgi, F., Solignac, S., Turon, J. L., Verleye, T., Wang, Y., Wang, Z. and Young, M.: Atlas of modern dinoflagellate cyst distribution based on 2405 data points, Rev. Palaeobot. Palynol., 191, 1–197, doi:10.1016/j.revpalbo.2012.08.003, 2013.

Zweng, M. M., Reagan, J. R., Antonov, J. I., Locarnini, R. A., Mishonov, A. V., Boyer, T. P., Garcia, H. E., Baranova, O. K., Johnson, D. R., Seidov, D. and 555 Biddle, M. M.: World Ocean Atlas 2013, Volume 2: Salinity, NOAA Atlas NESDIS, 74, 1–39 [online] Available from: http://www.bloodjournal.org/cgi/doi/10.1182/blood-2011-06-357442, 2013.
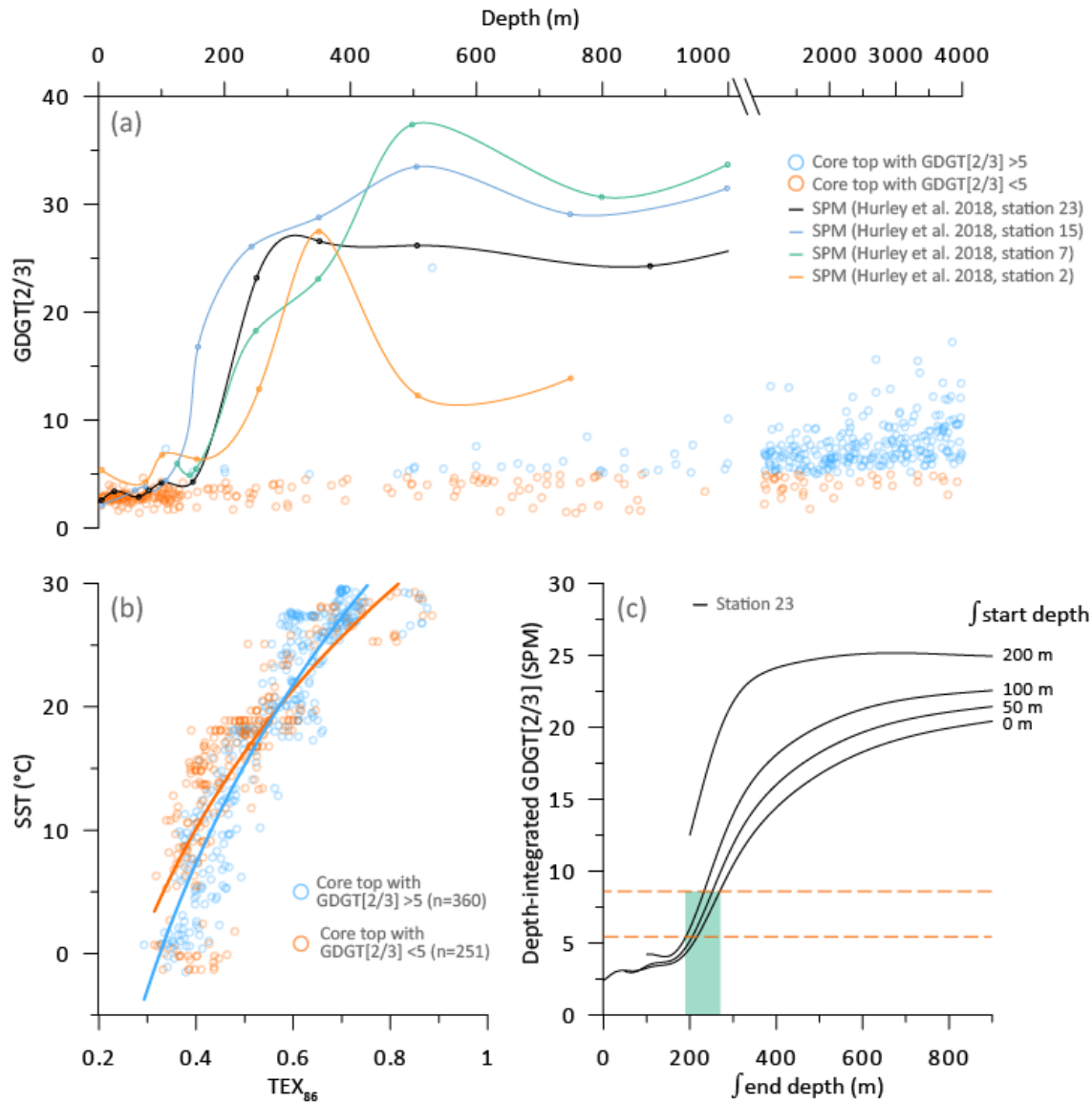
Figure 1. (a): Depth distribution of GDGT[2/3] ratio in suspended particulate matter (SPM; solid lines) at several stations in the Atlantic Ocean (Hurley et al., 2018) and in core tops (circles) between 65°N-65°S (Tierney and Tingley, 2015). **(b):** GDGT[2/3] vs. TEX_{86}, with logarithmic fits for GDGT[2/3]>5 (blue line) an GDGT[2/3]<5 (orange line). **(c):** Depth-integrated (linear) GDGT[2/3] from SPM data (station 23; Hurley et al., 2018). Integration start depths at 0 m, 50 m, 100 m and 200 m, and continuous end depth on x-axis. Range of typical Site 959 sedimentary GDGT[2/3] values between orange dashed lines, and corresponding range of potential integration end depths in vertical. Note that the assumed linear depth-weighing may not be realistic, but that an integration start depth at 200 m is incompatible with the sedimentary GDGT[2/3] values at Site 959, regardless of depth-weighing.
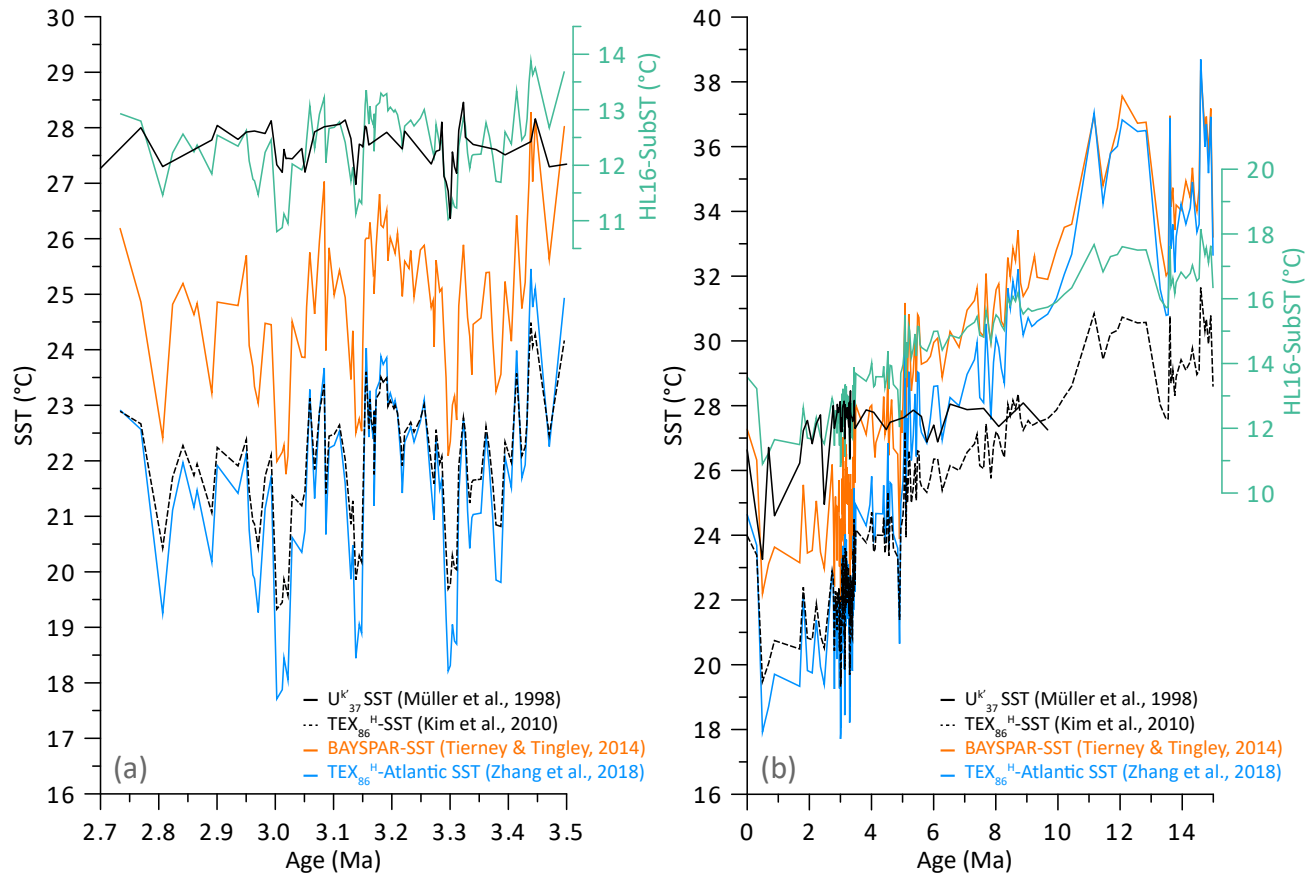
Figure 2. Site 959 TEX$_{86}$ record, calibrated using TEX$_{86}$^{H} and alternative SST calibrations and with the HL16-SubST calibration (Ho & Laepple, 2015), compared to the U$^{k'}_{37}$ record. Late Pliocene glacial-interglacial variability in (a), and 15 Myr evolution in (b).
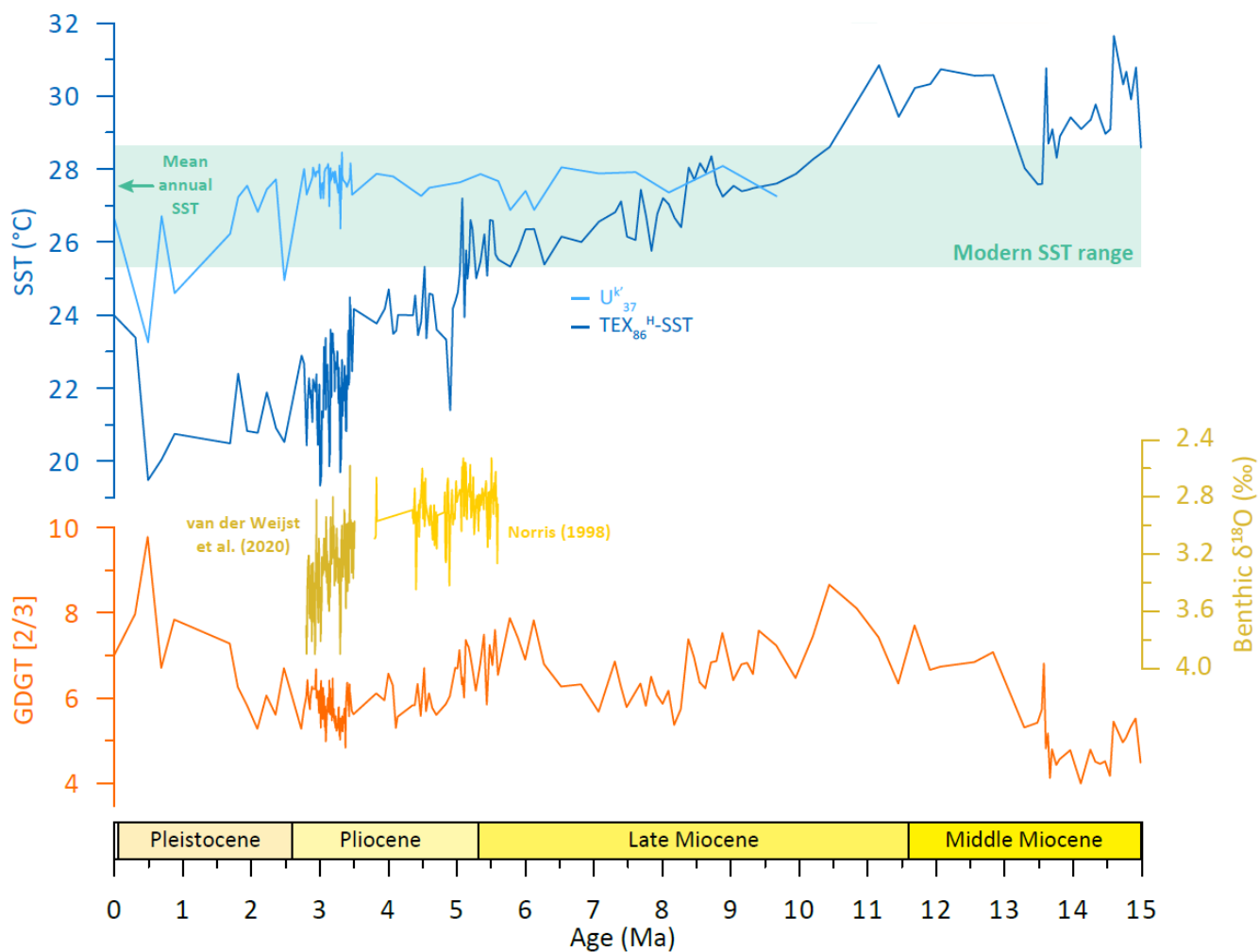
580

Figure 3. New TEX$_{86}^{H}$-SST (Kim et al., 2010 calibration), U$^{k'}_{37}$-SST (Müller et al., 1998 calibration) and GDGT[2/3] records at Site 959, compared to benthic δ^{18}O records from Norris (1998a) and van der Weijst et al. (2020). Shaded interval and arrow indicate annual SST range and mean annual SST in the Gulf of Guinea, respectively (Locarnini et al., 2013).
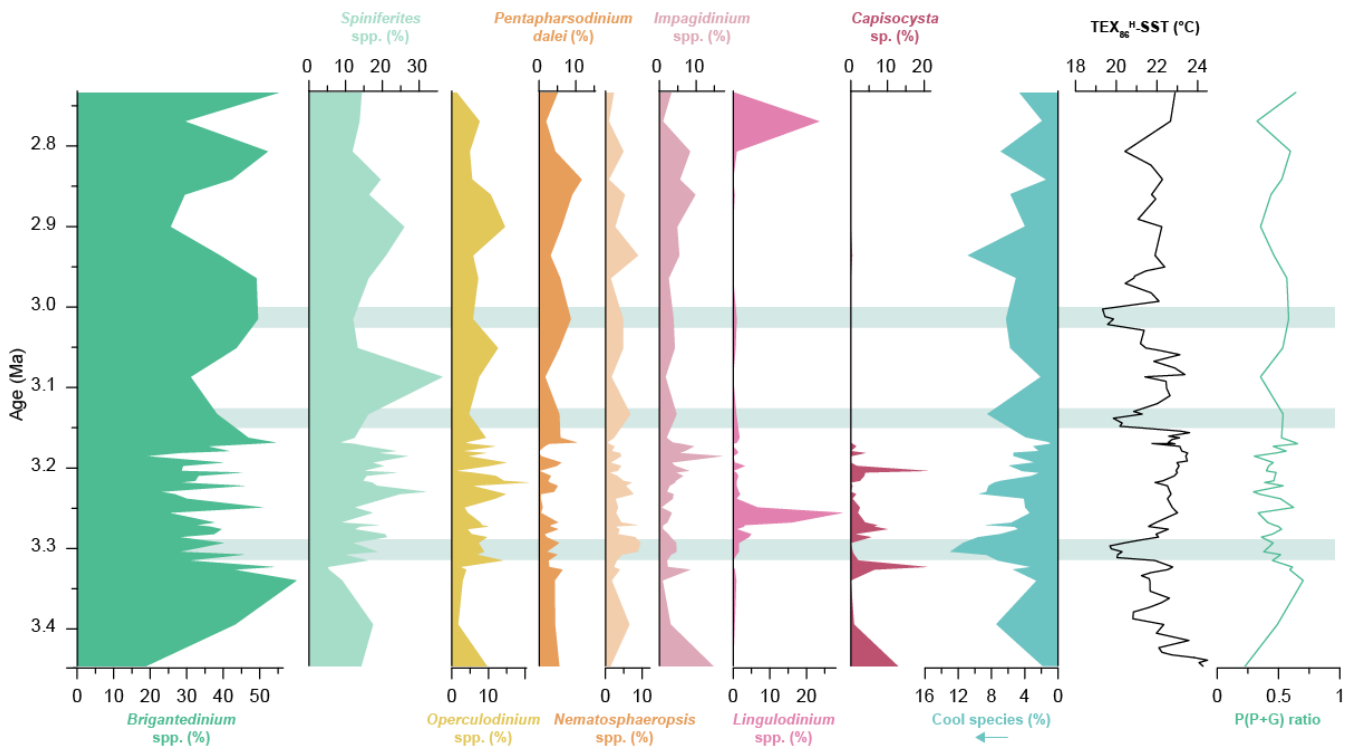
585

Figure 4. Relative abundances of the major groups of dinoflagellate cysts, the sum of dinocysts with cold affinities ("Cool species"), and P/(P+G) paleoproductivity index compared to TEX$_{86}^{H}$-SST. Shaded bands indicate TEX$_{86}^{H}$-SST minima during the late Pliocene M2, KM2 and G20 glacials.

590
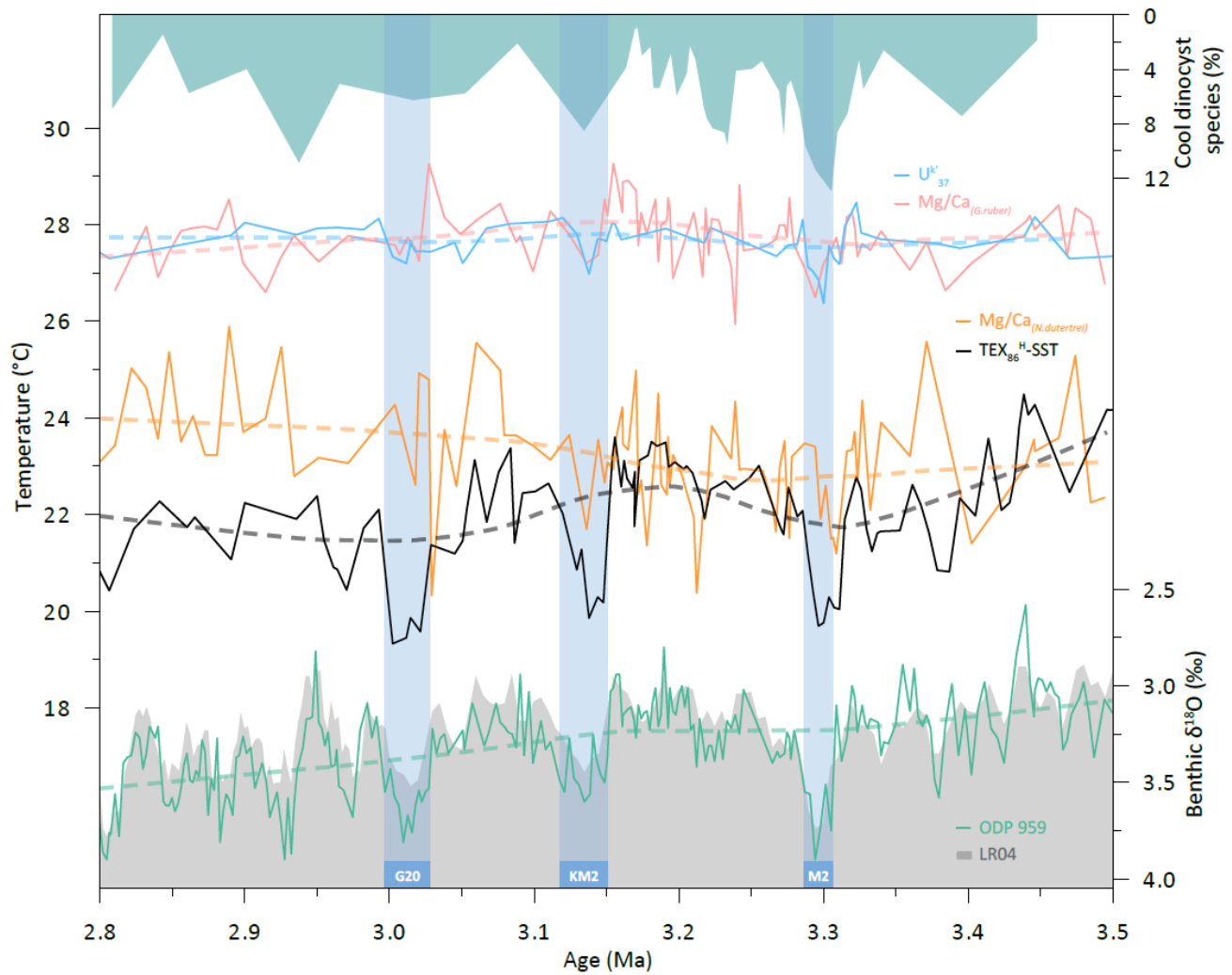
Figure 5. Compilation of late Pliocene multi-proxy temperature data and benthic δ¹⁸O at Site 959. Mg/Ca$_{(G.ruber)}$ (pink) and Mg/Ca$_{(N.dutertrei)}$ (yellow) from van der Weijst et al. (2022), benthic δ¹⁸O from van der Weijst et al. (2020) and LR04 δ¹⁸O stack (Lisiecki and Raymo, 2005) for reference. Dashed lines in are LOESS smoothed trends and vertical bands indicate the M2, KM2 and G20 glacial stages.
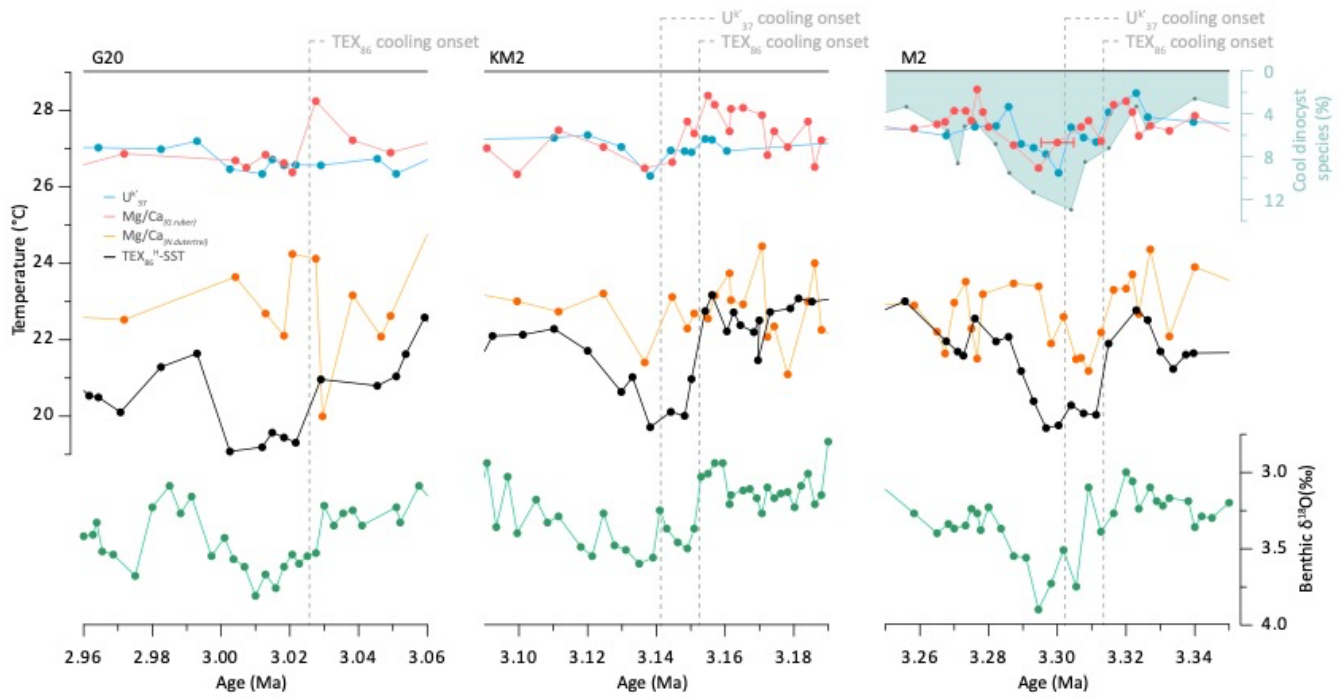
Figure 6. Close-up of G20, KM2 and M2 glacial stages in 100 kyr windows. Multi-proxy temperature data and benthic δ¹⁸O as in Figure 5. The resolution of the dinocyst record was too low for meaningful comparisons in KM2 and M2 glacials.
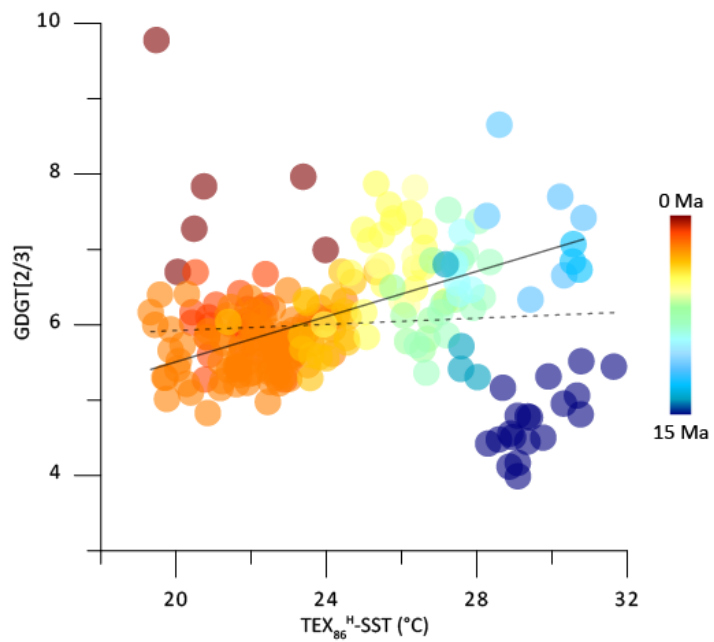
605

Figure 7. Cross-plot of TEX$_{86}^{H}$-SST and GDGT[2/3]. The oldest (>13.6 Ma; dark blue) and youngest (<1.7 Ma; dark red) samples largely stand out from the majority of the data. Linear regression lines determined from full dataset (stippled line) and samples dated between 13.6 and 1.7 Ma (solid line; 88% samples, R^2=0.37, p<0.001).
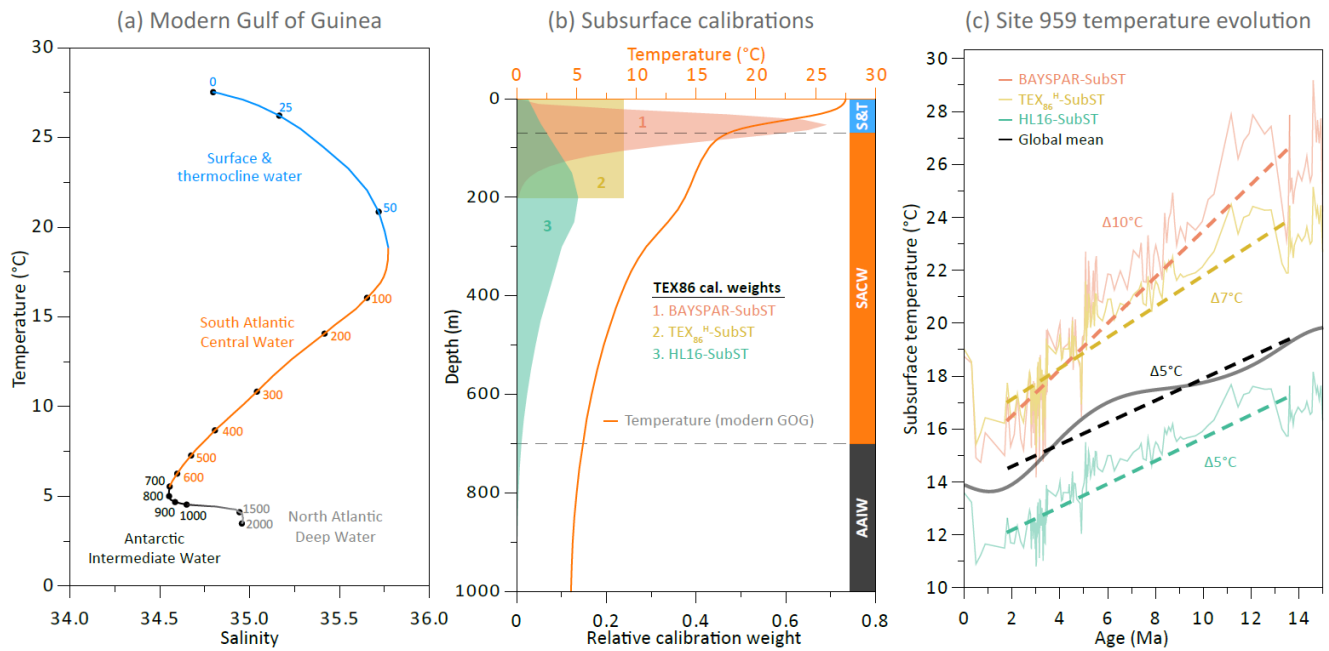
610

Figure 8. (a): Temperature and salinity distribution along a depth transect in the modern Gulf of Guinea (numbers: meters below sea surface), data from Locarnini et al., (2013) and Zweng et al., (2013). **(b):** Vertical weight distribution of the discussed SubST calibrations (silhouettes) and the water column composition in the modern Gulf of Guinea. **(c)** Site 959 TEX_{86}^{H}-SubST evolution according to different SubST calibrations, compared to global mean temperature evolution (Tierney et al., 2020). ΔTemperature estimated from linear trends (dashed lines) between the Middle Miocene and Pleistocene.

615

620
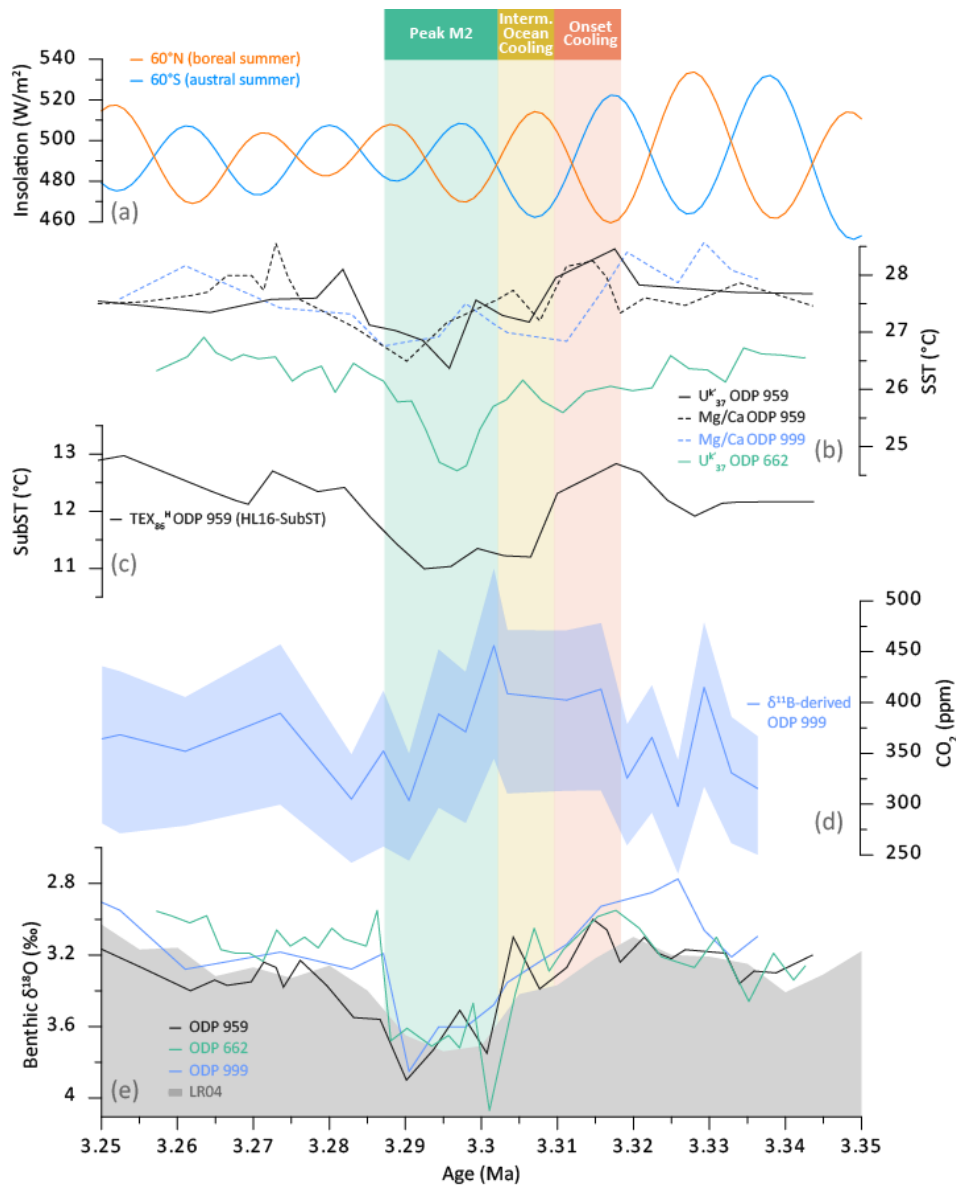
Figure 9. Exploring the chronology around the M2 glacial with records aligned on peak glacial benthic $\delta^{18}O$ values (original age models in Figure S2). (a): Daily insolation at 60°N/S during NH/SH summer solstice (Laskar, 1990). (b): East equatorial Atlantic SST at Site 959 (this study) and Site 662 (Herbert et al., 2010) and Caribbean Sea SST at Site 999 (de la Vega et al., 2020). (c): Site
625 **959 TEX_{86} HL16-SubST, indicative of intermediate ocean temperatures (d): Atmospheric CO_2 reconstructions from Site 999 (de la Vega et al., 2020). (e): Benthic $\delta^{18}O$ records of Site 959 (van der Weijst et al., 2020), 662 (Lisiecki and Raymo, 2005) and 999 (Haug et al., 2001; de la Vega et al., 2020), aligned to LR04 (Lisiecki and Raymo, 2005) on peak M2 values.**